

# Finding the Weight Difference of a Rectangular Structure with a Parabolic Arc for Mathematical Models Made of Steel and other Composite Materials

TYMOR ABED ALSTTAR SEDIQER<sup>1</sup>, EMAD TOMA KARASH<sup>2\*</sup>, JAMAL NAYIEF SULTAN<sup>3</sup>,  
MAJID KHALEEL NAJEM<sup>3</sup>

<sup>1</sup>Department of Civil Technologies, Kirkuk Technical Institute,  
Northern Technical University,  
Mosul 41000,  
IRAQ

<sup>2</sup>Department of Mechanical Technology, Mosul Technical Institute,  
Northern Technical University,  
Mosul 41000,  
IRAQ

<sup>3</sup>Department of Power Mechanical Engineering, Technical Engineering College,  
Northern Technical University,  
IRAQ

*Abstract:* - The most popular materials for lightweight constructions, including building and aircraft structures, industrial, military, and aerospace technology, are armored composites. Composites made of carbon fiber are typically employed in lightweight applications. The ANSYS program was used to produce four mathematical models. Steel is used in the construction of the first and second versions whereas composite materials are used in the third and fourth variants. To find all the deformations, stresses, and strains that appear on the four models, as well as to calculate the weights of those four structures and compare them, these four models were tested with the ANSYS 15.0 program to obtain equal deformation resistance for all models under the influence of different loads. The results show that the composite models had lower strains, stresses, and deformations than the steel models. Among other results, it was discovered that the weight of the third model made of composite materials decreased by (32.72%) compared to the steel-based first model, and after doing the necessary calculations and assessing the results, the fourth model made of composite materials' weight was reduced by (19.21%) when compared to the second model made of steel.

*Key-Words:* - Steel, Parabolic arc, Carbon fiber, Composite materials, Beams, Finite element method.

Received: March 7, 2023. Revised: July 27, 2023. Accepted: September 8, 2023. Published: September 28, 2023.

## 1 Introduction

High-strength steel is increasingly being used in construction, and steel is a common building element. When utilized for vertical members in high-rise structures, high-strength steel can efficiently minimize cross-sectional size, maximize space utilization, and save material costs. The most often utilized form of steel in engineering is that which is limited by ties. The ties-confined concrete stress-strain relationship is taken into consideration while analyzing the mechanical characteristics of high-strength steel vertical members.

In several engineering disciplines, such as shipbuilding, aviation, and civil engineering, thin

plates are structural components that are frequently utilized. Ship plates with ribs and stiffeners, offshore panels, and aerospace panels are frequently used and always subject to partial edge traction on their plane. This kind of loading may cause buckling, which has a detrimental effect on how well the involved structural elements function. In-plane compression and shear loads can result in regional or global plate instability. The corrugations that emerge from plate instability could cause lasting damage to the entire structure and lead it to lose efficiency given analytical solutions in their research of thin plate buckling under compression and shear, [1], [2].

The three most important requirements for the structural frame of buildings and other projects are strength, stiffness, and stability. However, one of the key challenges in creating logical and economical constructions is the development of effective structural elements with the right bearing capacity and ideal size. This challenge is solved using a variety of generic algorithm options, topological optimization, the theory of adaptive optimization, and other techniques, [3], [4], [5], [6]. In many areas of technology, including mechanical engineering, aircraft engineering, instrument engineering, and construction, topological and parametric optimization techniques are applied to create the best possible construction projects, [7], [8], [9], [10]. Studies have shown that the use of fiber-reinforced pile-reinforced polymer systems in the building, construction, and industrial fields to externally strengthen concrete sections and pipes is a practical alternative. The effectiveness of these systems has been confirmed by numerous experimental experiments, [11], [12], [13]. Due to their lower dead weight than reinforced cement composites, composite structures are substantially less susceptible to seismic conditions. Currently, high-rise structure design and construction research employs cutting-edge techniques, a variety of design software, and sophisticated experimental techniques to get reliable results. This is accomplished by taking into account both the task benefits of using steel reinforcement and the advantages of using various types of concrete. These elements have an impact on the composite columns' high capacity and axial compression, despite their various shapes, [14], [15], [16]. Advanced composite materials with excellent mechanical properties and low specific weight make up the majority of today's thin-walled contractions. Materials with thin stiffening walls are the major focus. They are created and constructed as closed or open profiles with intricate slatted shapes and different shapes, [17], [18], [19], [20], [21], [22]. The stirrups and steel coil in SRC columns may be able to handle the internal concrete deformation and strength. The impact of stirrups having concrete borders has been extensively researched, [23], [24], [25]. Epoxy resin composites have been a mainstay in the engineering and industrial fields for a good while. Parts with superior mechanical, thermal, and electrical ties have been created using epoxy-based component manufacturing, [26]. To enhance the characteristics of epoxy resins, it is now customary to add a second phase (such as inorganic fillers). Recent studies have demonstrated that carbon fiber-reinforced polymer-based composites greatly enhance the mechanical,

thermal, and barrier properties of pure polymer matrices, [27], [28]. Matrix strengthening is undoubtedly one of the procedures used to enhance the compressive and flexural properties of composites made from fiber fabrics, [29]. It has been demonstrated that a polymer matrix's mechanical characteristics can be greatly improved by the addition of a tiny quantity of stiff nanoparticles, [30], [31].

The goal of this article is to develop composite material structures for buildings, halls, and warehouses that are resistant to deformations, stresses, and strains at levels comparable to those found in steel structures under the same loads. Along with other requirements like resistance to corrosion, vibrations, and fatigue stresses to which it is exposed, halls, warehouses, etc., are also included.

## 2 Materials and Model Analysis

The four three-dimensional models of the four various types of beams were made using the ANSYS-15 program. The first and second models are built of traditional materials (steel), whereas the third and fourth models are made of composite materials. The upper surfaces of the two models (M1 and M3) are precisely subjected to a 50 kN force along the y-axis. A distributed load was applied from above along all top structures and at a value of (2308 N/m) for the two models (M2 & M4). Figure 1 shows the shapes and dimensions of the fourth model.

Describe the mechanical characteristics of steel, epoxy resin, and carbon fiber composition in Table 1. The results of the all mechanical properties of the composite materials as calculated using the Mathcad-15 program are shown in Table 2. Table 3 shows the models, codes, specific disciplines, element types, and load types used.

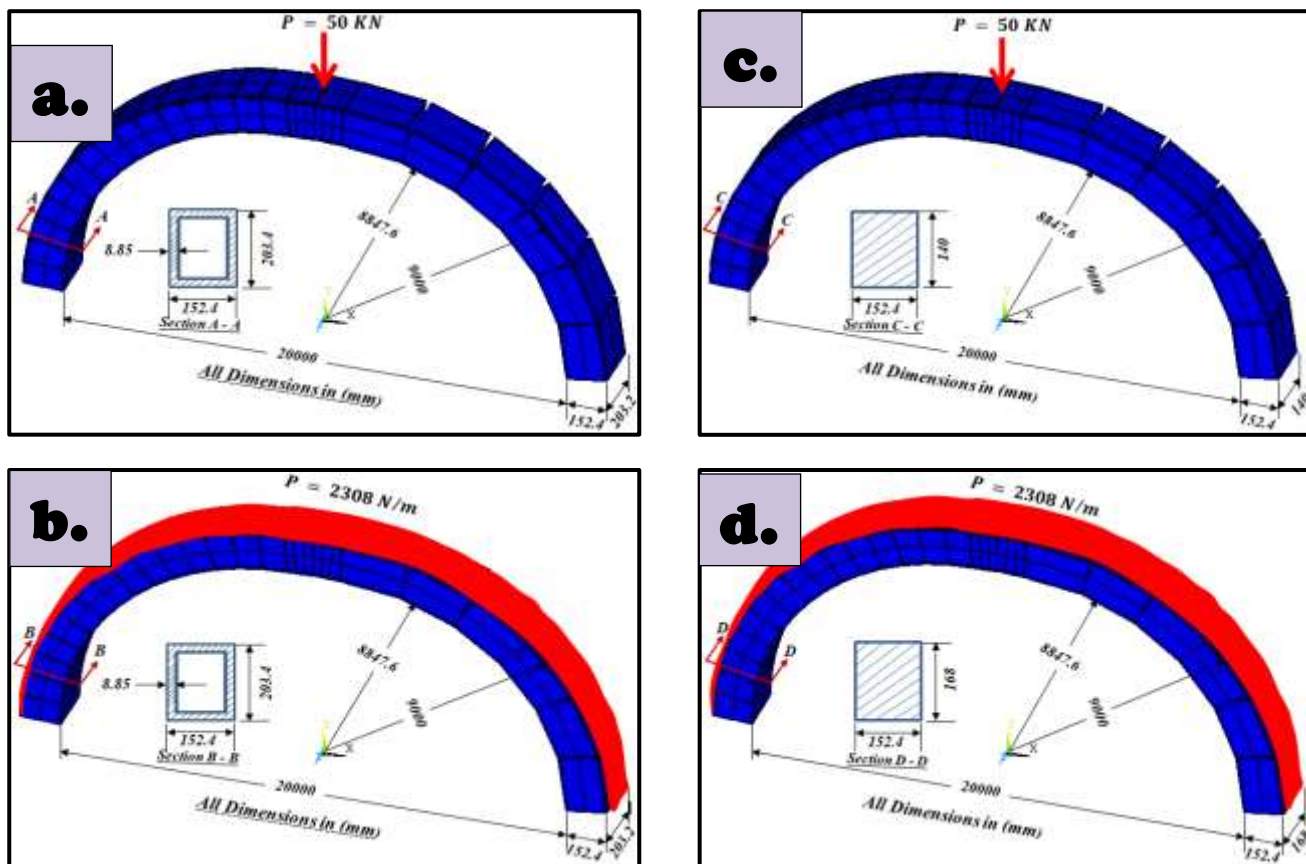


Fig. 1: It indicates the model form, cross-sectional area, and dimensions used in the tests

Table 1. Describe the mechanical characteristics of steel, epoxy resin, and carbon fiber, [32], [33]

Model	Materials	Density, $\rho$ , ( $Kg/m^3$ )	Modulus of Elasticity, $E$ , (GPa)	Passion's Ratio	Modulus of Rigidity, $G$ , (GPa)	Price Kilograms, \$	
M-1	Steel	7870	205	0.3	80		
M-2							
M-3	T300 Carbon Fiber and 7901 Epoxy Resin	T300 carbon fiber, 40 %	1765	125	0.24	5.43	14
M-4		7901 Epoxy Resin, 60 %	1299	11.3	0.31	3.98	0.05

Table 2. The findings of the composite materials' mechanical properties as determined

Models	Materials	Code used in Mathcad-15 program [0]			Code used in Mathcad-15 program [90]		
		$E_{ii}$ , (MPa)	$G_{ij}$ , (MPa)	$\mu_{ij}$	$E_{ii}$ , MPa	$G_{ij}$ , (MPa)	$\mu_{ij}$
Model - 3	T300 Carbon Fiber and 7901 Epoxy	$E_{11} = 107600$	$G_{12} = 13870$	$\mu_{12} = 0.232$	$E_{11} = 196100$	$G_{12} = 10970$	$\mu_{12} = 0.051$
Model - 4		$E_{22} = 149200$	$G_{13} = 35730$	$\mu_{13} = 0.281$	$E_{22} = 58170$	$G_{13} = 6997$	$\mu_{13} = 0.281$
		$E_{33} = 113200$	$G_{23} = 21740$	$\mu_{23} = 0.281$	$E_{33} = 110900$	$G_{23} = 4054$	$\mu_{23} = 0.301$

Table 3. Models, codes, Individual disciplines, element types, as well as the several load types

No.	Model	Code	Individual - Disciplines	Type of Element	Loads
1	Model -- 1	-----	Structural	Beam 188	50 KN
2	Model -- 2	-----	Structural	Beam 188	2308 N/m
3	Model -- 3	[0/90] <sub>70</sub>	Structural	SHELL 281	50 KN
4	Model -- 4	[0/90] <sub>84</sub>	Structural	SHELL 281	2308 N/m

### 3 Results and Discussion

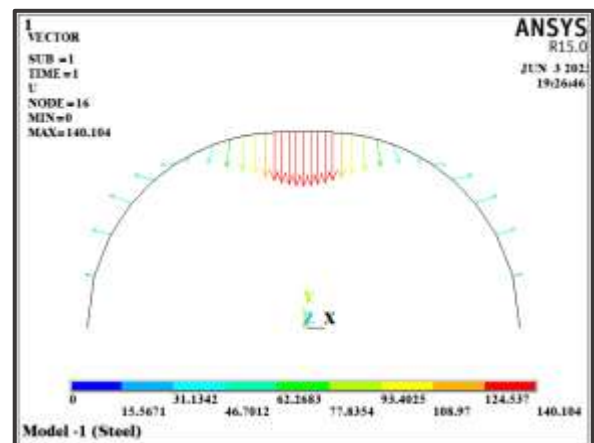
A curved column of the same length was designed for four different mathematical models, the first and second models of steel with a hollow section, and the third and fourth models of composite materials with a solid section. Loads were applied to the four models using the ANSYS program. Where a load of (50 KN) was applied as shown in Figure 1-a on the first model. The results of deformations, strains, and stresses that appeared on the model were obtained, as the value of deformation was (140.104 mm).

In the second model, Figure 2-b, a distributed load was applied to the model from its beginning to its end. Many simulations were carried out by reducing the load, to obtain a load that results in the same deformation obtained in the first model, whose value was (140.104 mm). After making several attempts to change the applied load, a load that achieves this was obtained, and the value of this load was (2308 N/m).

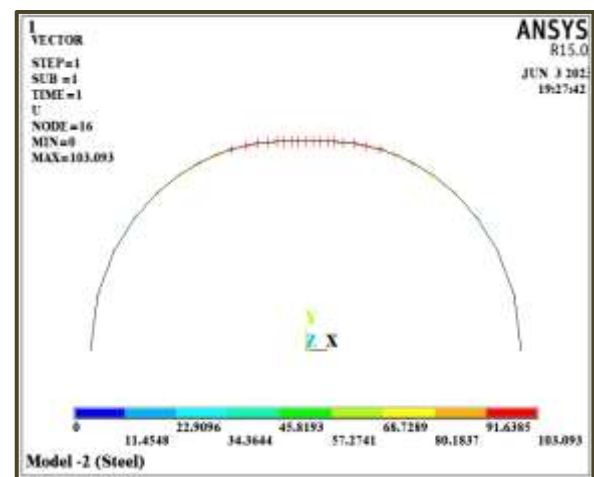
After designing the third model consisting of composite materials, the same load was applied in the first model, whose value was (140.104 mm). The number of layers was changed and the results were extracted to the stage of obtaining the same deformation in the first model, after making quite a few attempts. The same deformation was obtained in the first model, which was (140.104 mm). This was achieved when the number of layers reached (140 layers), and each layer had a thickness of (1 mm). In the fourth model, which is also composed of composite materials, the same load was applied to the second model, whose value was (140.104 mm). The number of layers was changed until a deformation equal to the deformation in the other models was obtained. After conducting a large number of attempts using the ANSYS 15.0 program, the optimal solution was obtained, in which the number of layers consisting of the arched column reached (168 layers).

Figure 2, Figure 3, Figure 4, Figure 5, Figure 6, Figure 7, Figure 8, Figure 9, Figure 10, Figure 11, Figure 12, Figure 13, Figure 14, Figure 15, Figure 16 and Figure 17 shows all the results obtained through the four model tests under the influence of

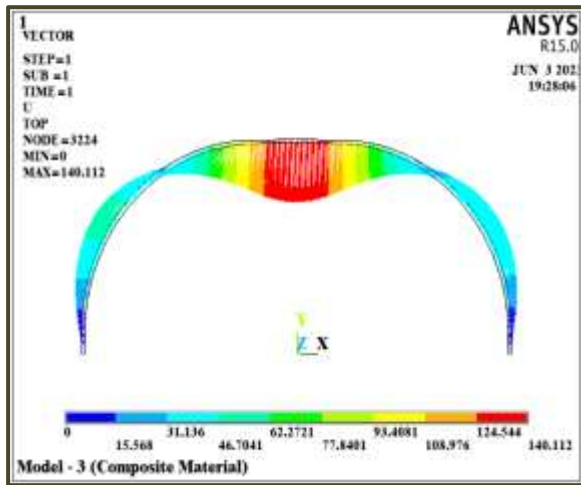
the loads applied to them. These figures show the deformations, stresses, and strains that appeared on the four models after loads were applied to them, by using the ANSYS program.



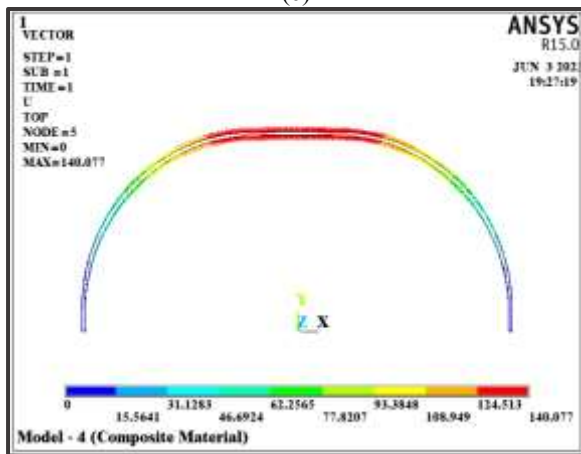
(a)



(b)

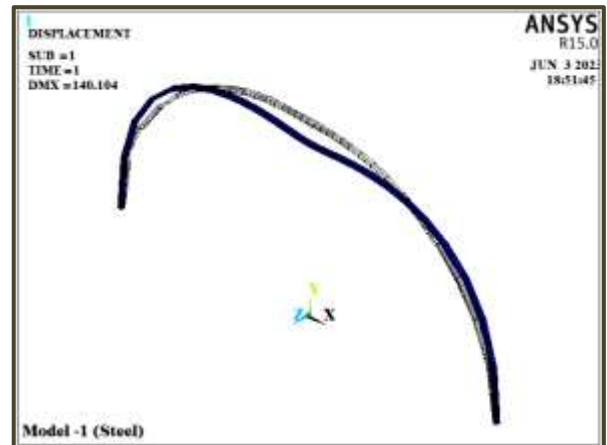


(c)

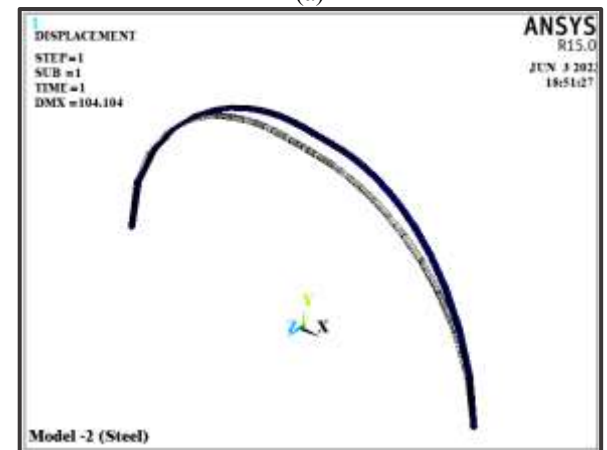


(d)

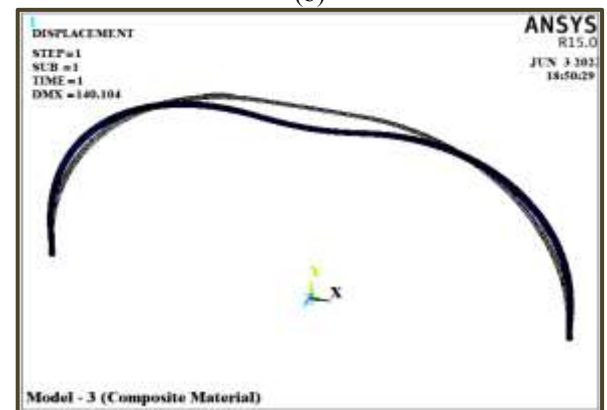
Fig. 2: The displacements ( $S$ ) distribution across all models



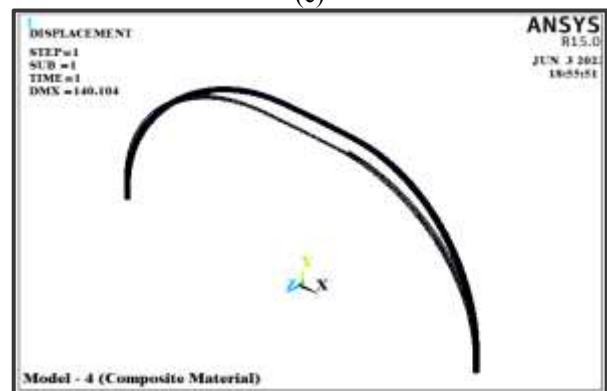
(a)



(b)

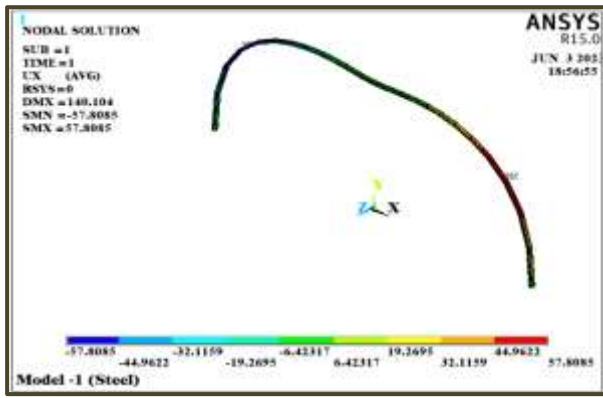


(c)

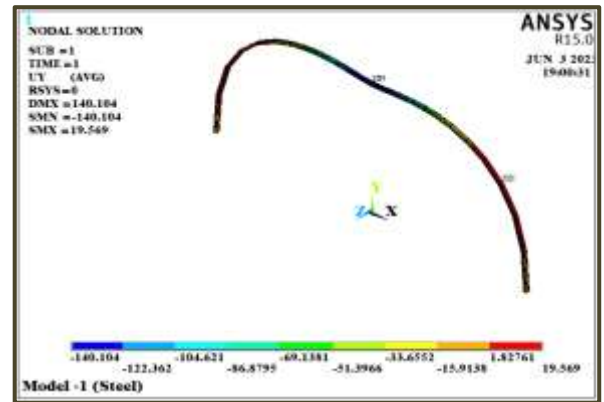


(d)

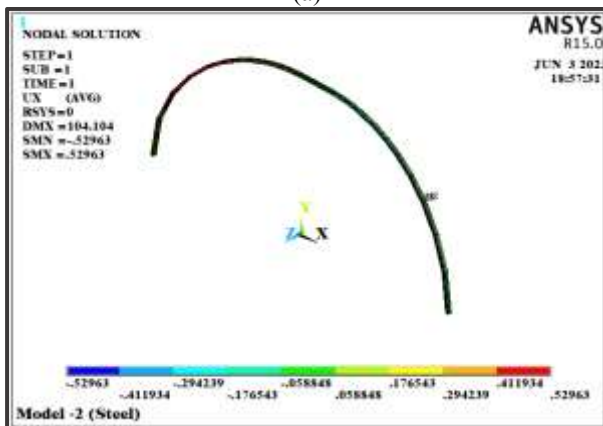
Fig. 3: The deflections ( $\delta$ ) results across all models



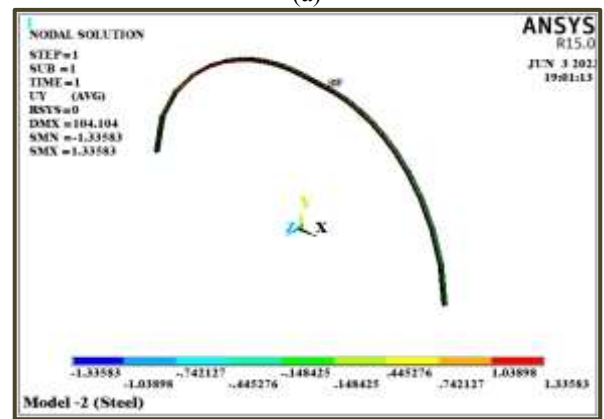
(a)



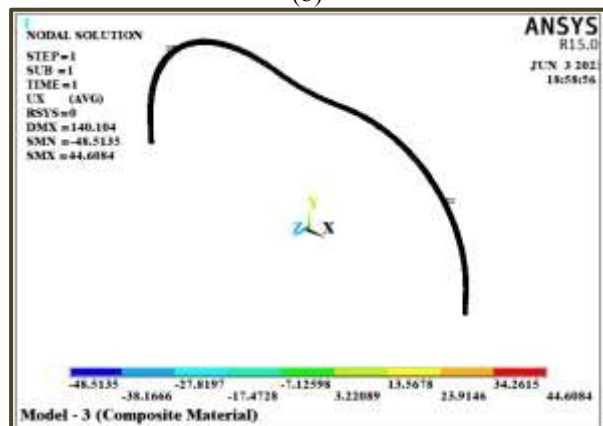
(a)



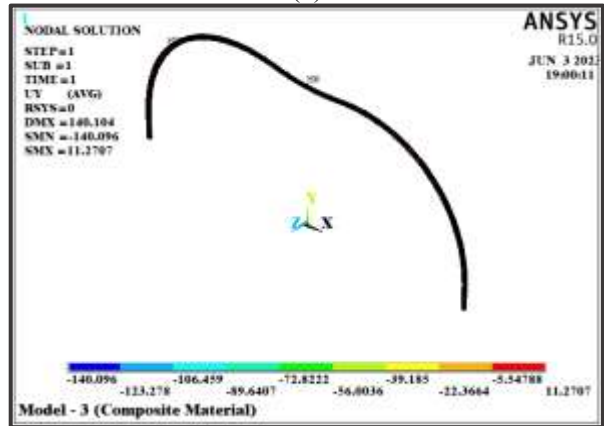
(b)



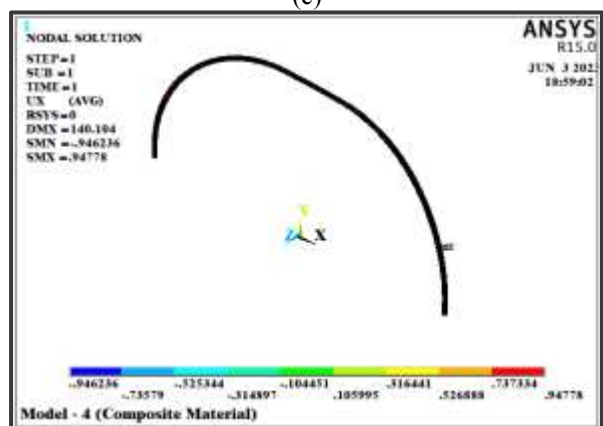
(b)



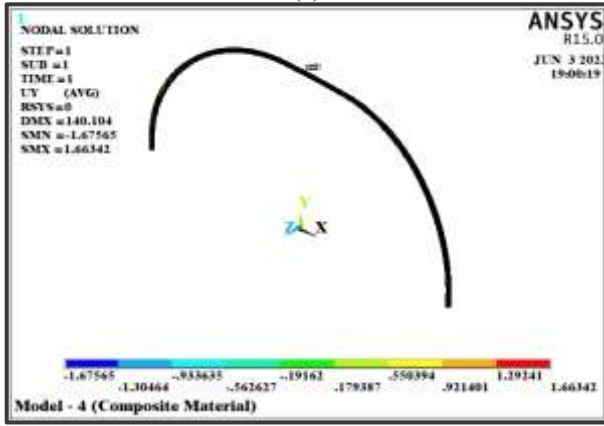
(c)



(c)



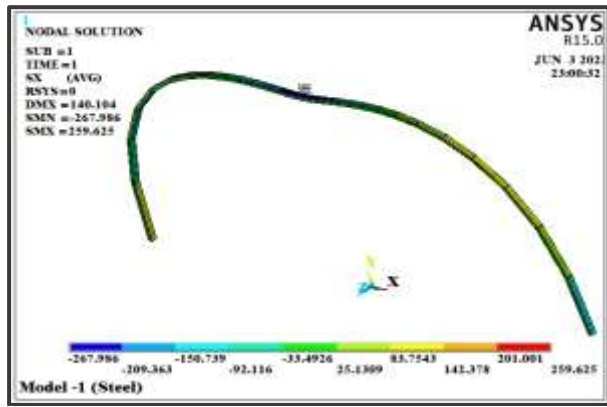
(d)



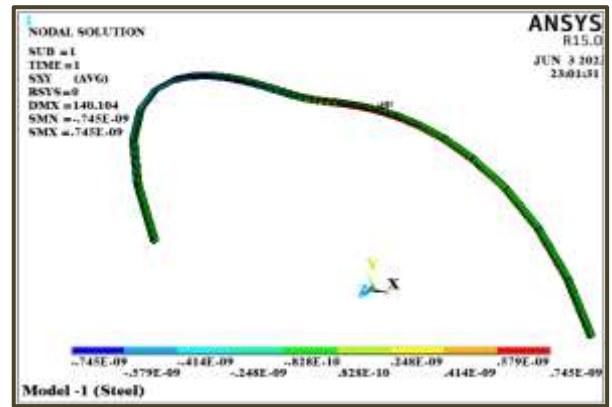
(d)

Fig. 4: The displacements ( $U_x$ ) results across all models

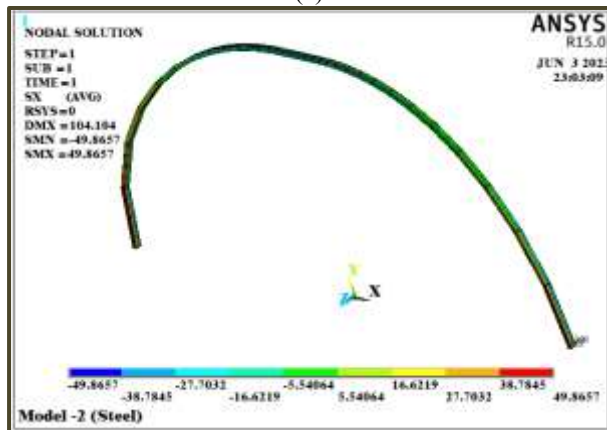
Fig. 5: The displacements ( $U_y$ ) results across all models



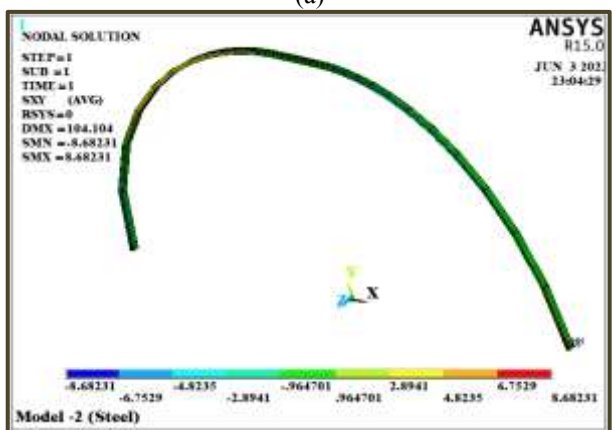
(a)



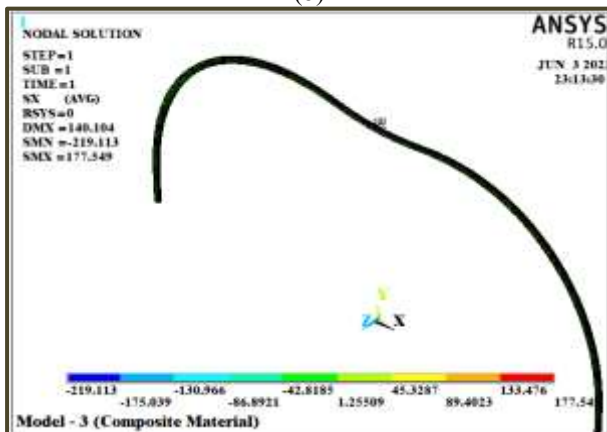
(a)



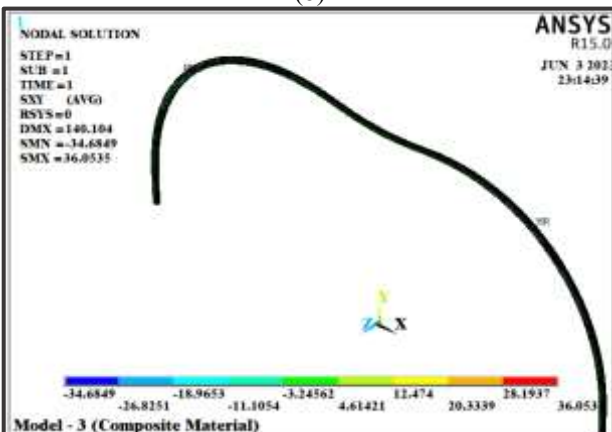
(b)



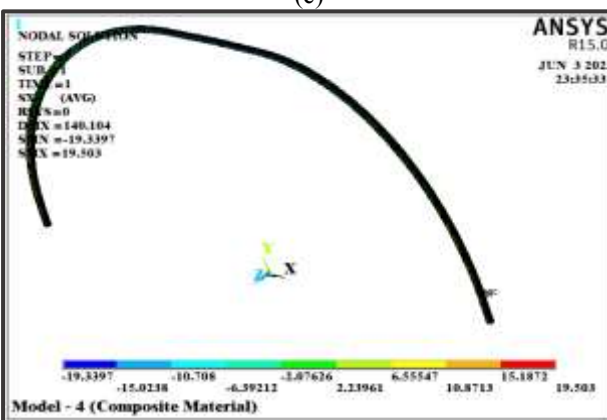
(b)



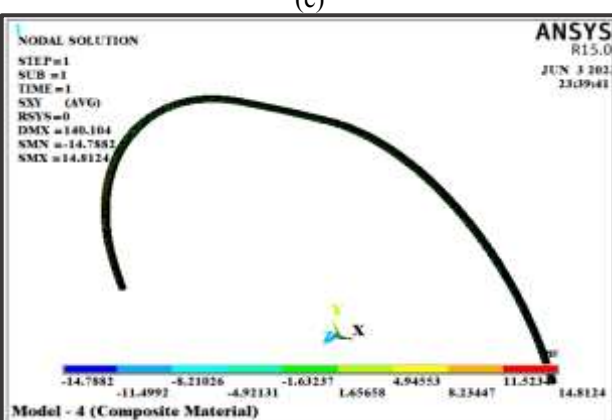
(c)



(c)



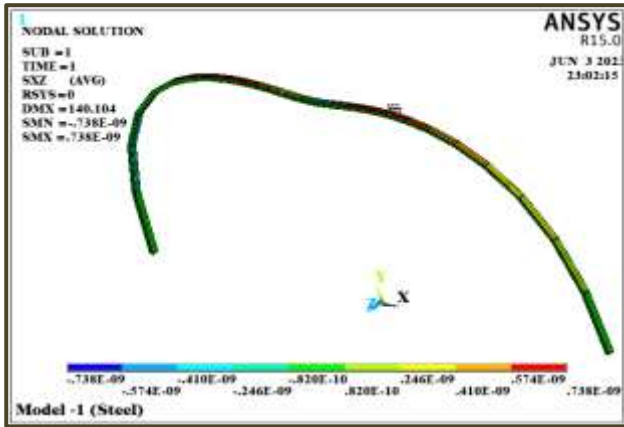
(d)



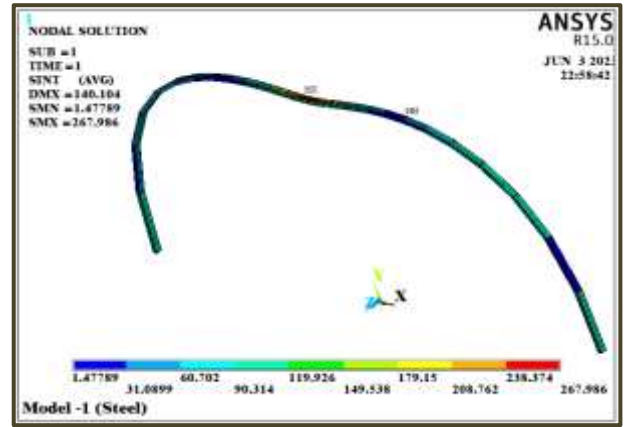
(d)

Fig. 6: The normal stresses ( $\sigma_x$ ) results across all models

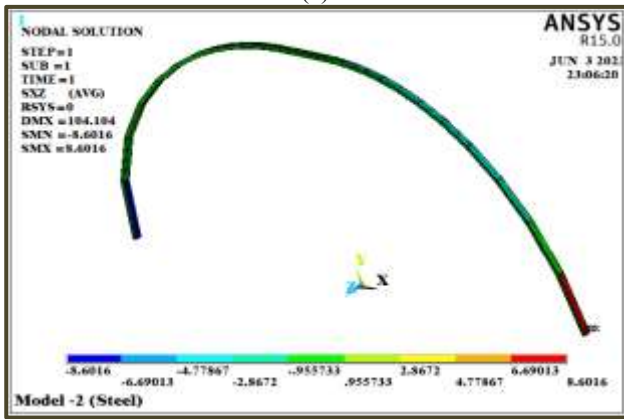
Fig. 7: The shear stresses ( $\tau_{xy}$ ) results across all models



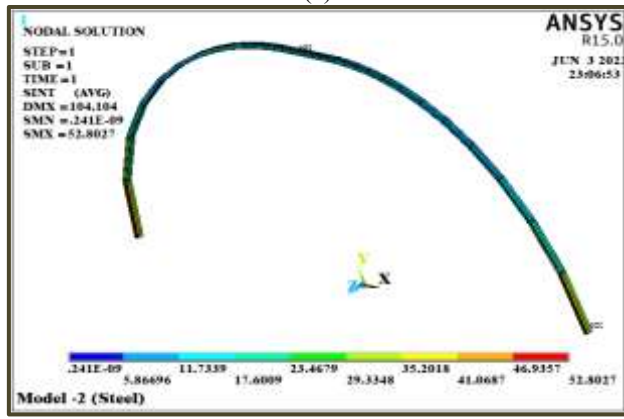
(a)



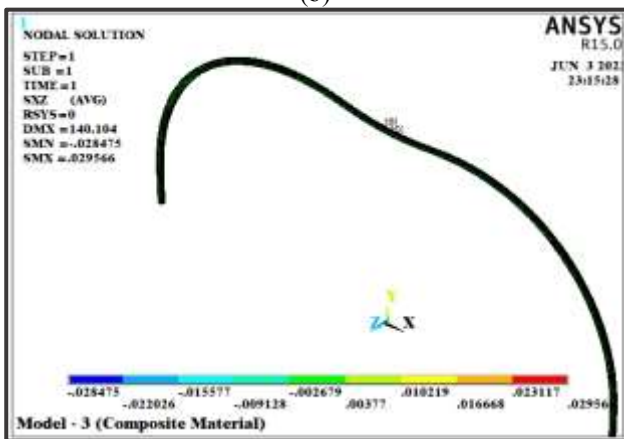
(a)



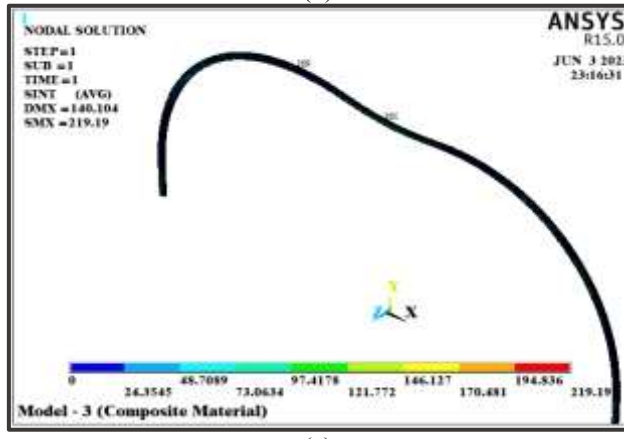
(b)



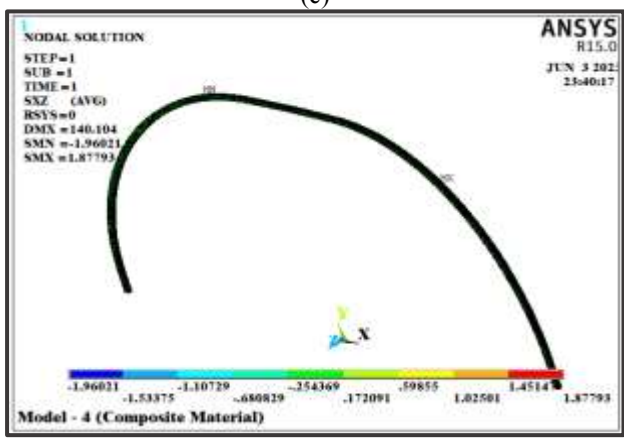
(b)



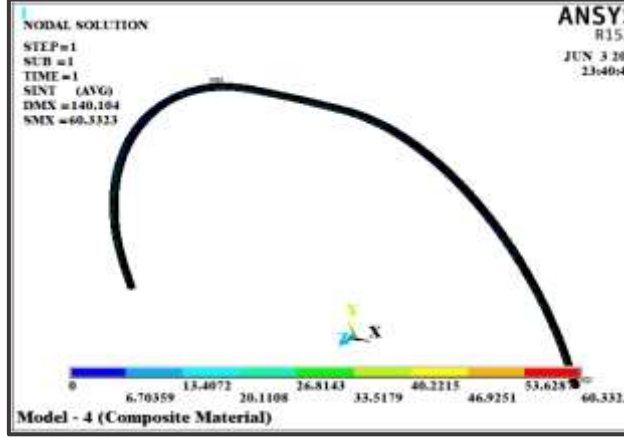
(c)



(c)



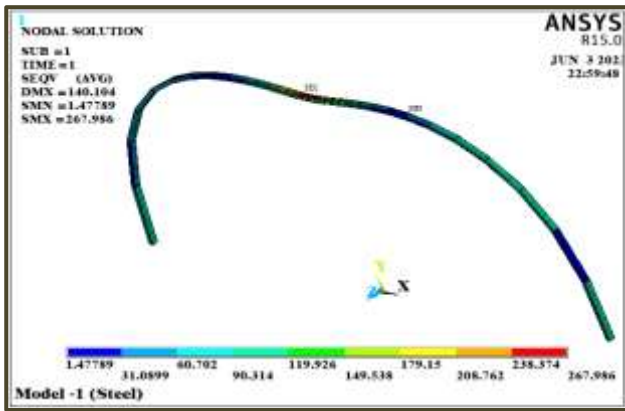
(d)



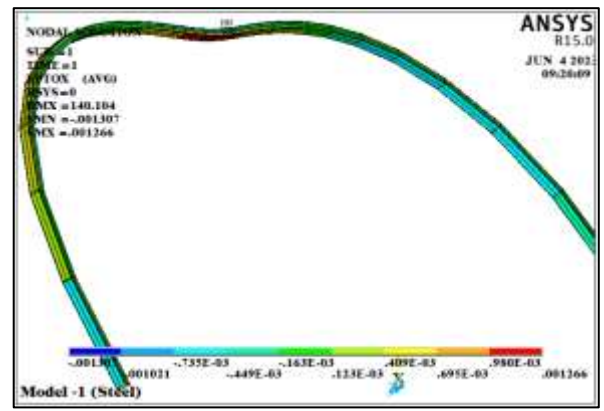
(d)

Fig. 8: The shear stresses ( $\tau_{xz}$ ) results across all models

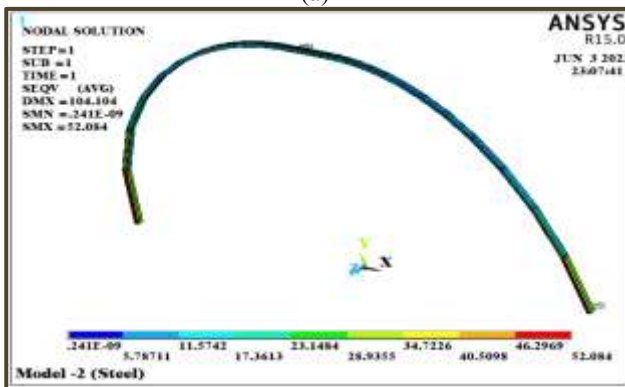
Fig. 9: The intensity stresses ( $\sigma_{int}$ ) results across all models



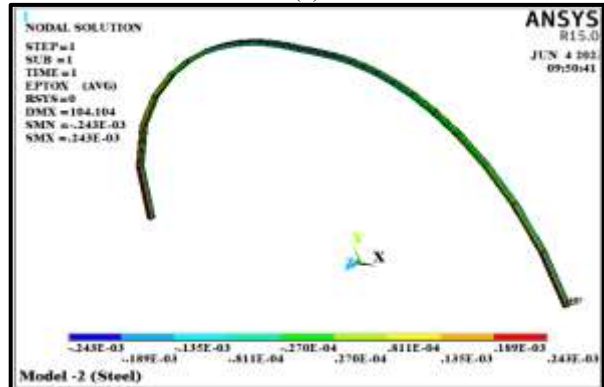
(a)



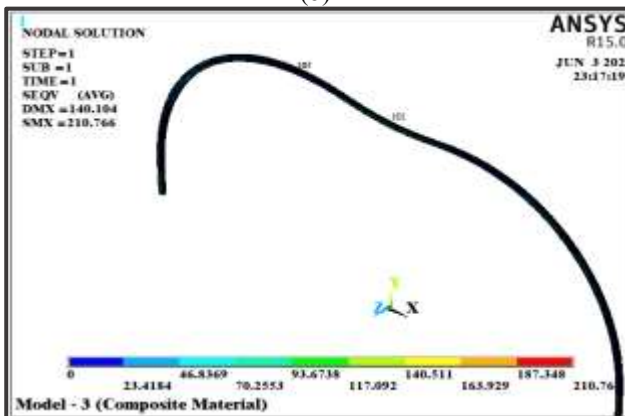
(a)



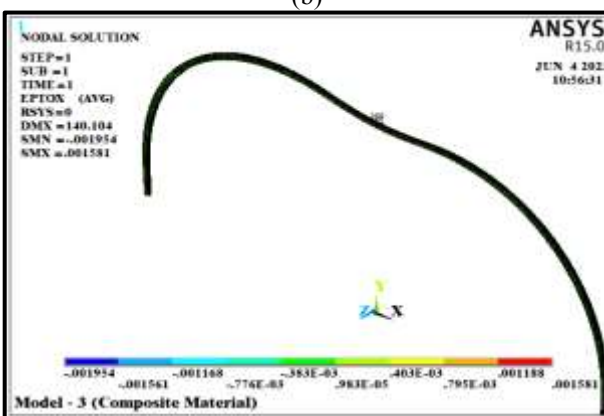
(b)



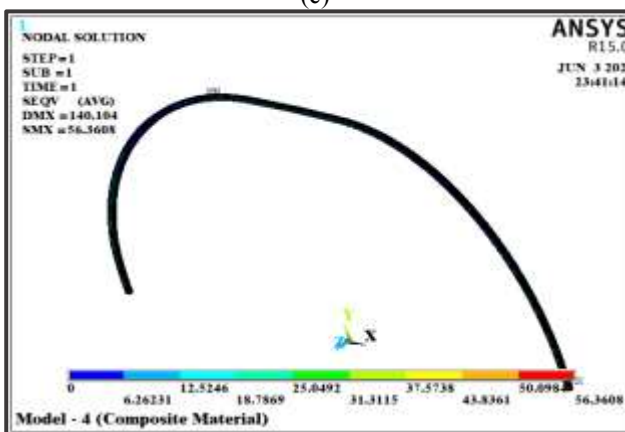
(b)



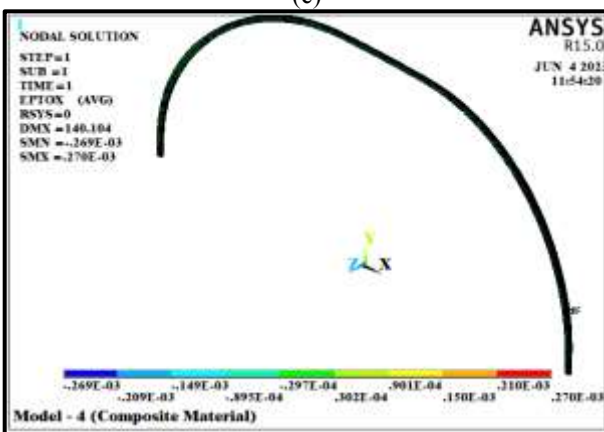
(c)



(c)



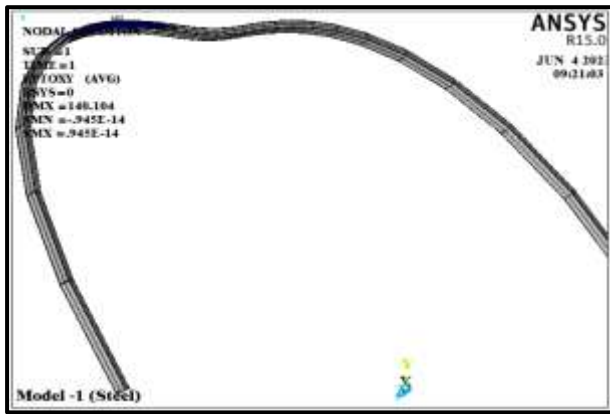
(d)



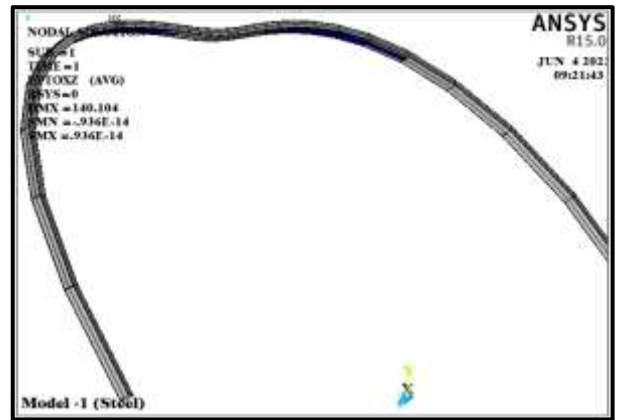
(d)

Fig. 10: The intensity stresses ( $\sigma_{von}$ ) results across all models

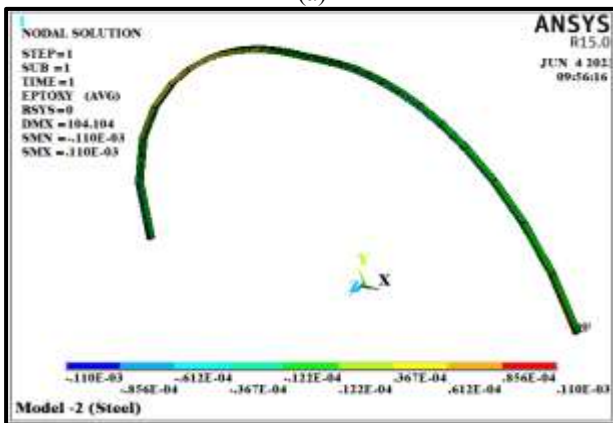
Fig. 11: The normal strains ( $\epsilon_x$ ) results across all models



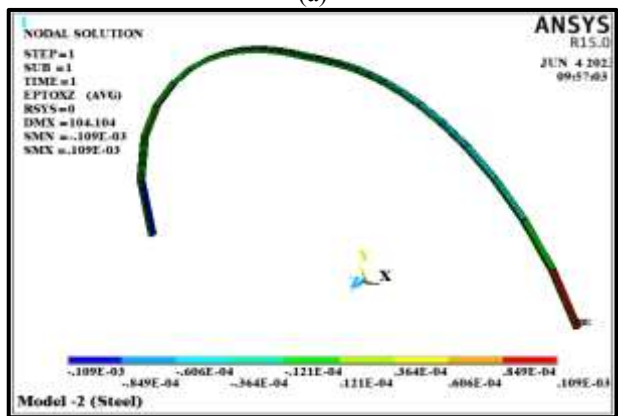
(a)



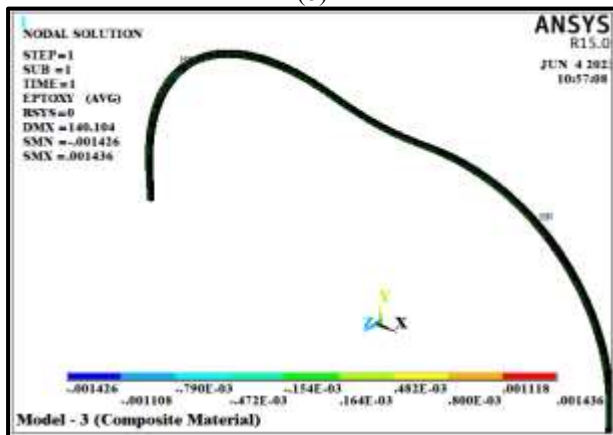
(a)



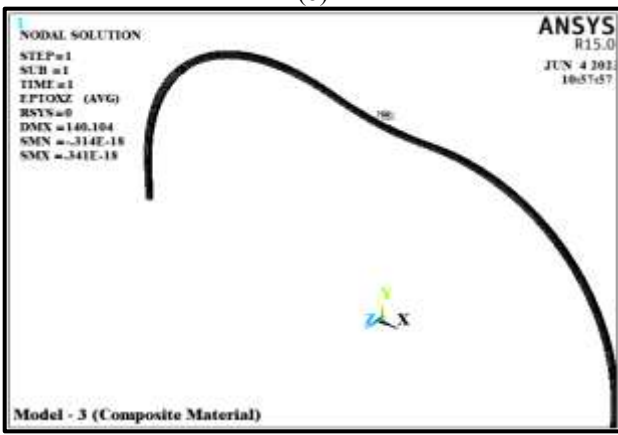
(b)



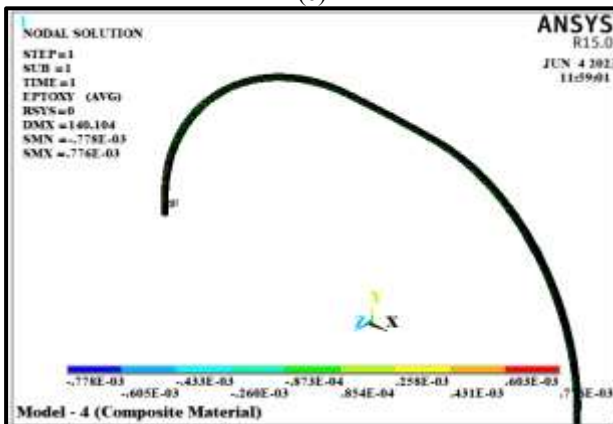
(b)



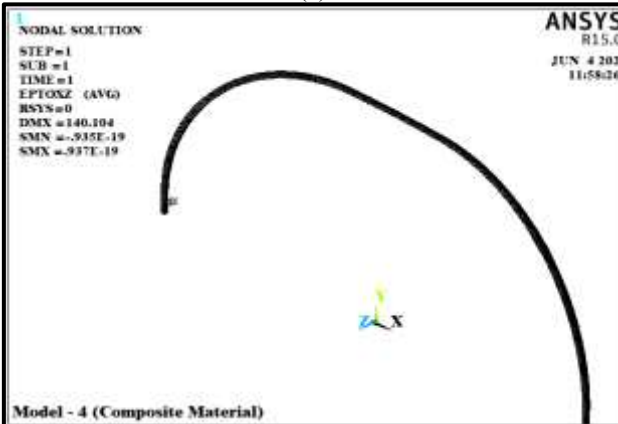
(c)



(c)



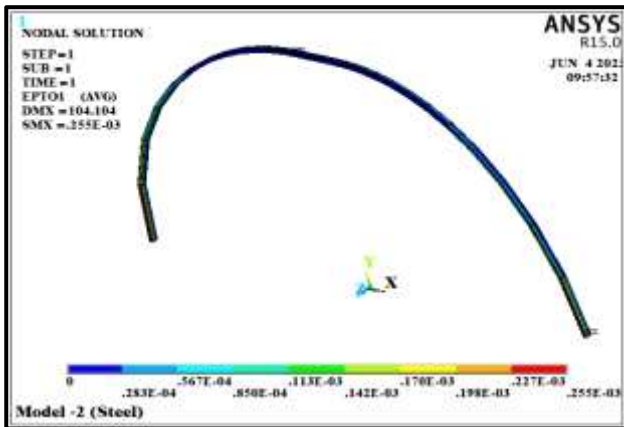
(d)



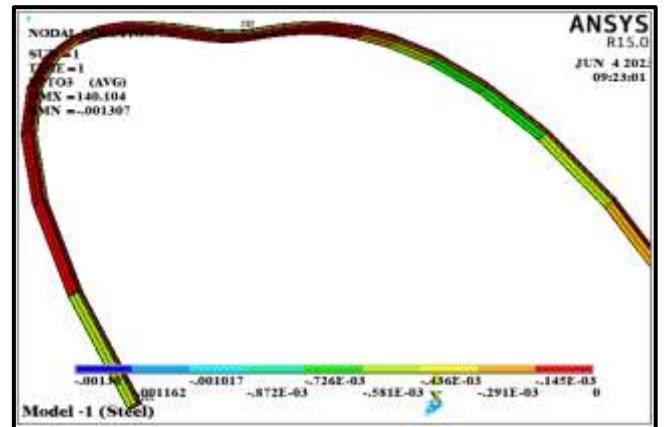
(d)

Fig. 12: The shear strains ( $\epsilon_{xy}$ ) results across all models

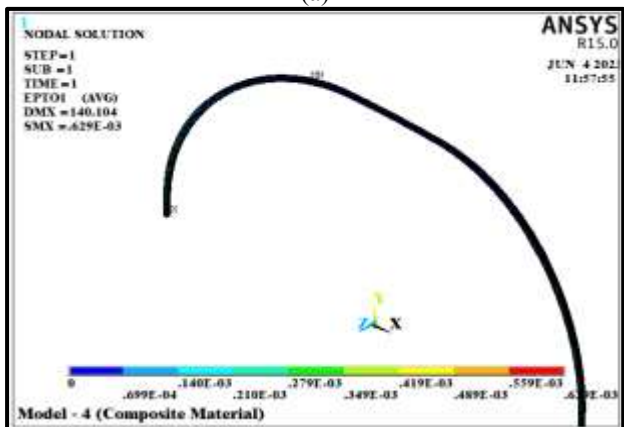
Fig. 13: The shear strains ( $\epsilon_{xz}$ ) results across all models



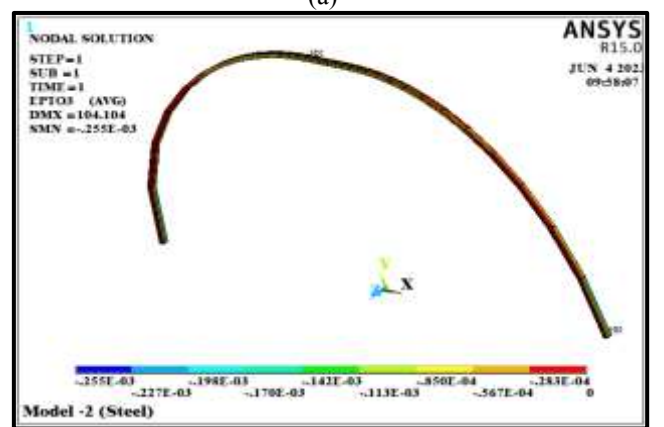
(a)



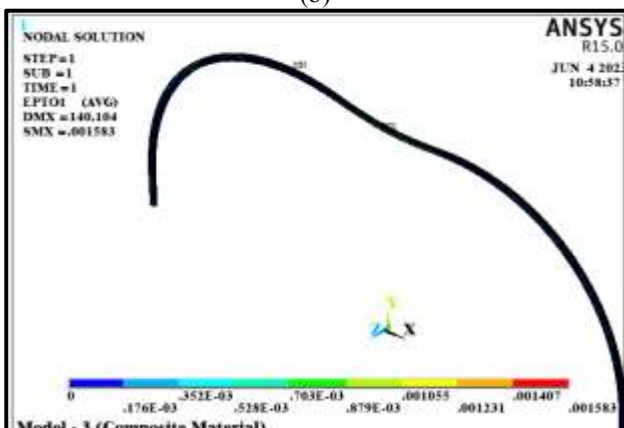
(a)



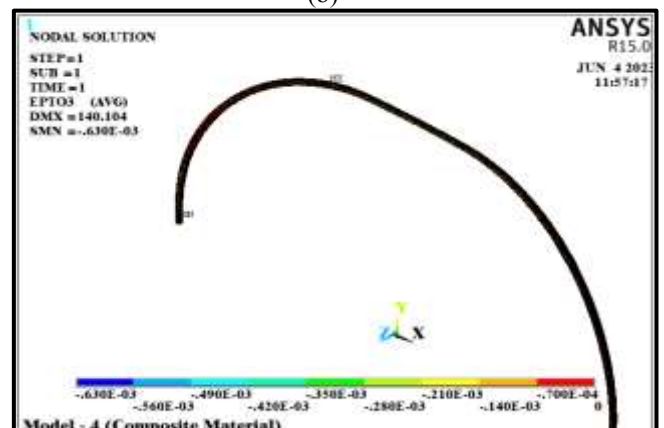
(b)



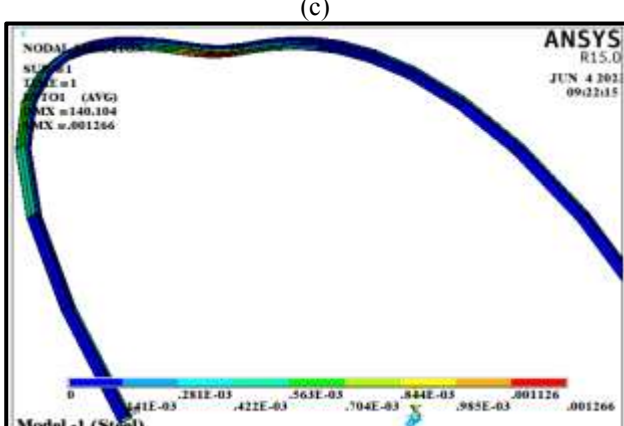
(b)



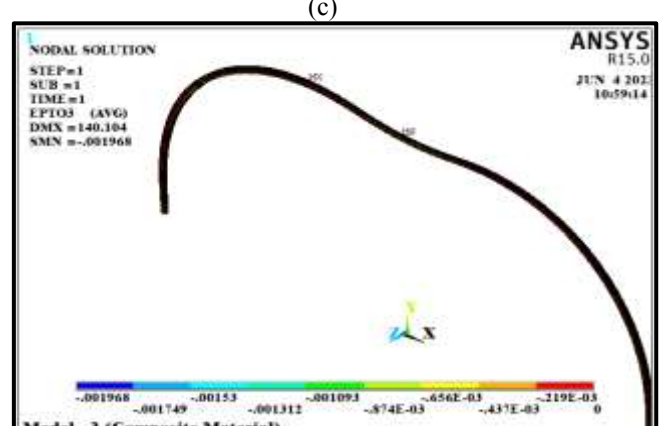
(c)



(c)



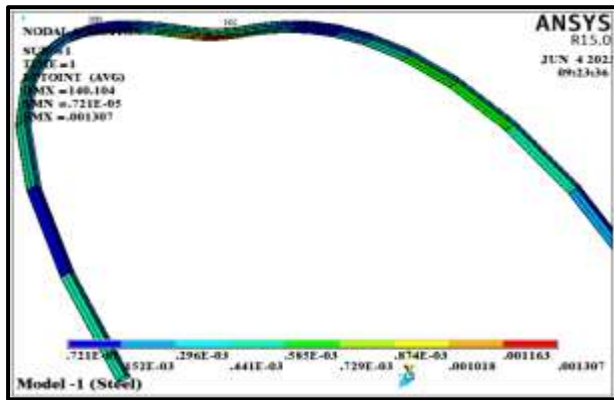
(d)



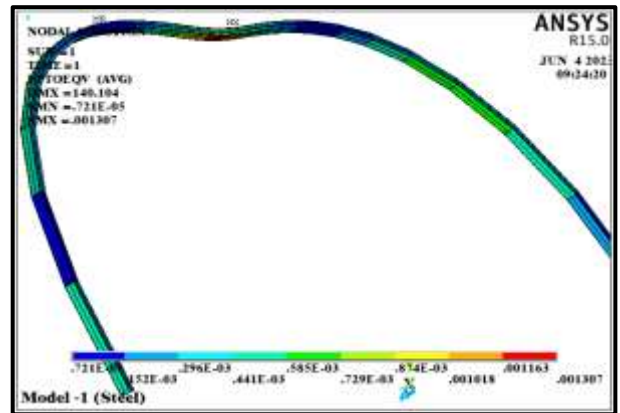
(d)

Fig. 14: The first strain ( $\epsilon_{first}$ ) results across all models

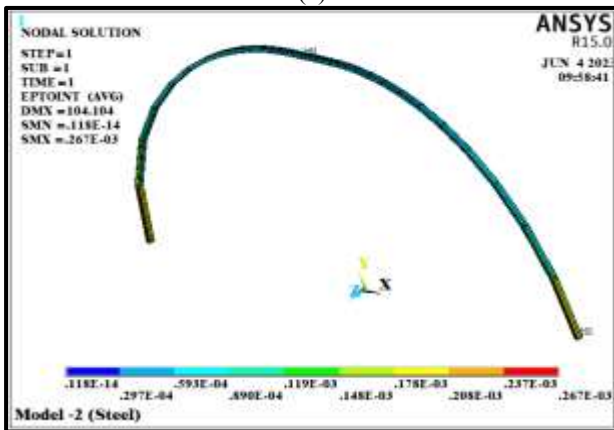
Fig. 15: The third strain ( $\epsilon_{third}$ ) results across all models



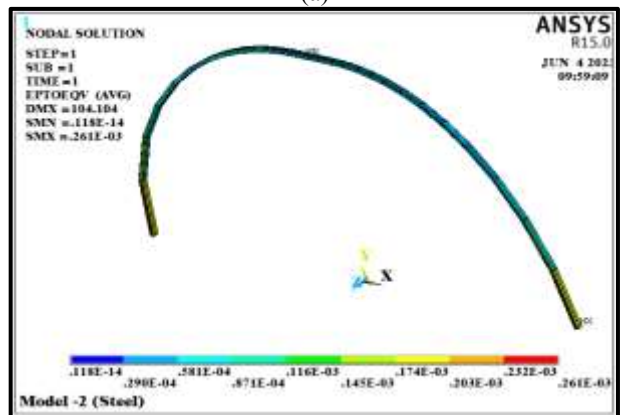
(a)



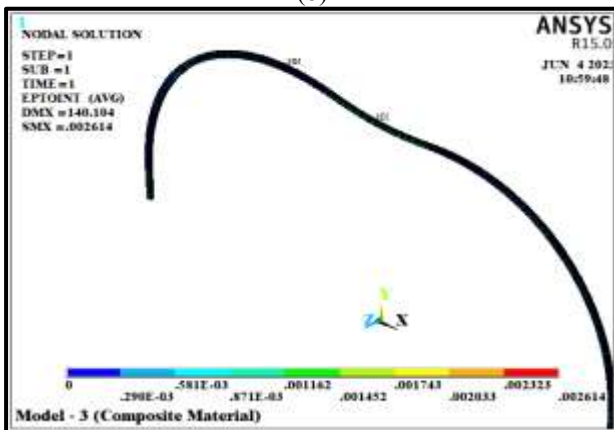
(a)



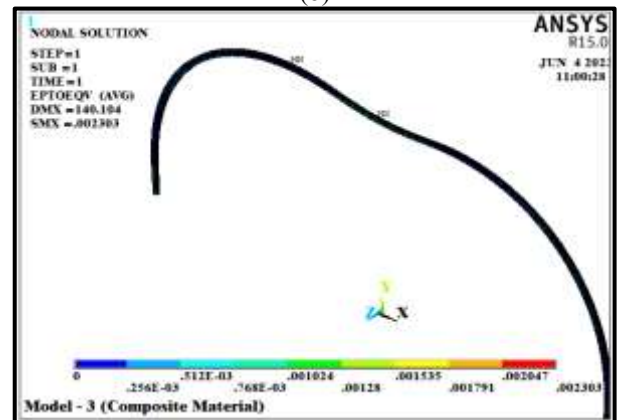
(b)



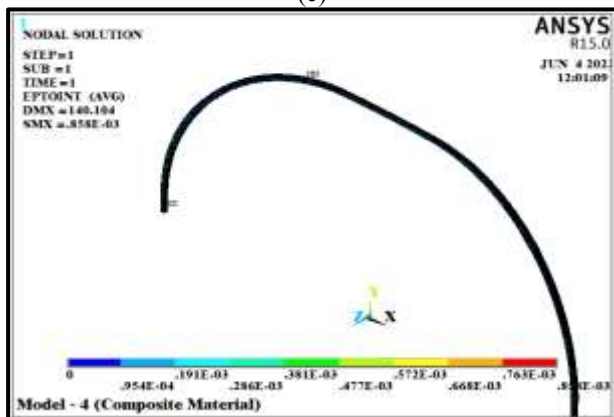
(b)



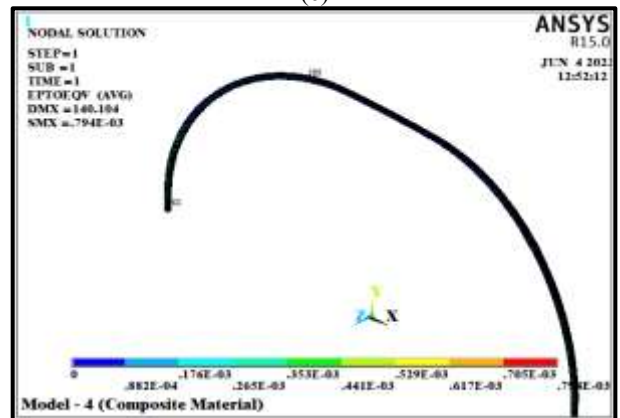
(c)



(c)



(d)

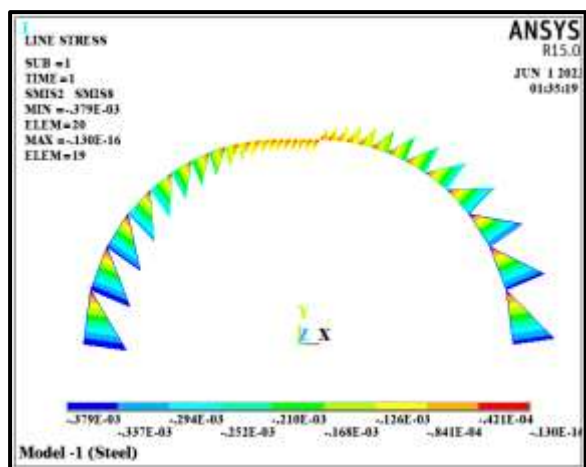


(d)

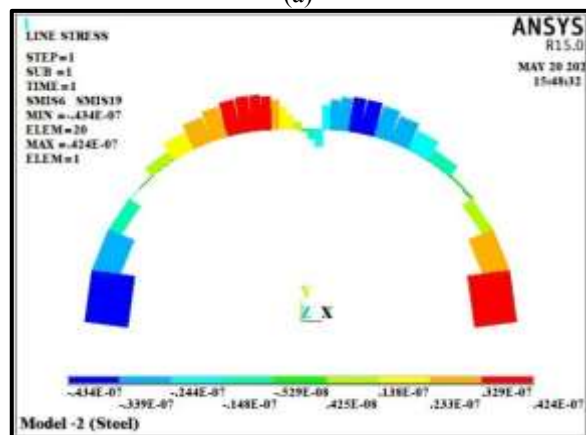
Fig. 16: The intensity strains ( $\epsilon_{int.}$ ) results across all models

Fig.17: The von strains ( $\epsilon_{von.}$ ) results across all models

Figure 18 displays the load distribution on the first and second models as well as the shape of the load distribution and the places with the highest shear forces. The maximum bending moment is shown in Figure 19, along with the distribution of moments on the first and second models and where it occurs.

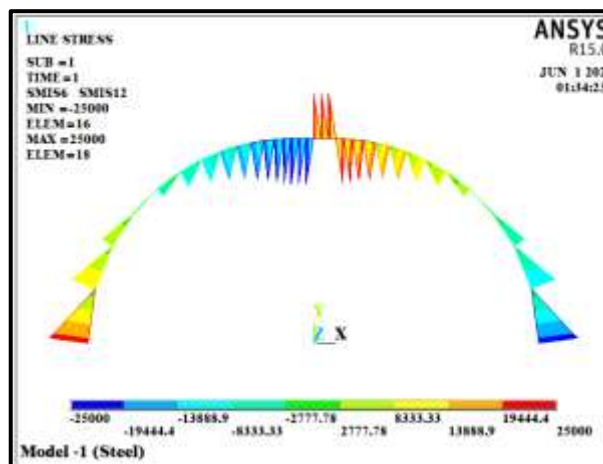


(a)

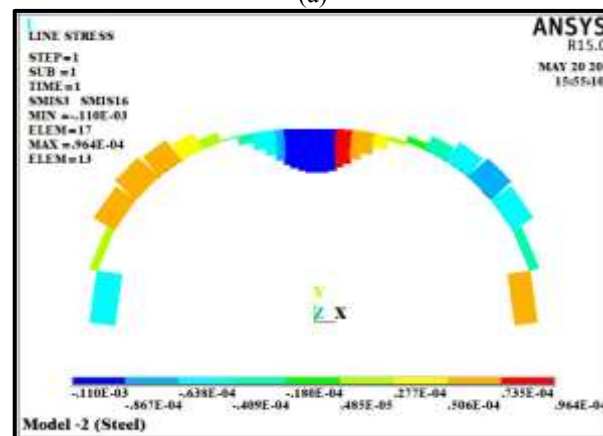


(b)

Fig. 18: The shear forces ( $S-F$ ) results, for models (1, 2)



(a)



(b)

Fig. 19: The bending moments ( $B - M$ ) results, for models (1, 2)

Based on the deformations, stresses, and strains that appeared on the models after loading, the ANSYS program's results for the four models are summarized in Table 4.

Table 4. A summary of the findings from stress, strain, and deformations on the four models is displayed

No.	Model	$\delta$ (mm)	$U_x$ (mm)	$U_y$ (mm)	$\sigma_x$ (MPa)	$\tau_{xy}$ (MPa)	$\tau_{xz}$ (MPa)	$\sigma_{int.}$ (MPa)	$\sigma_{von}$ (MPa)	$\epsilon_x$	$\epsilon_{xy}$	$\epsilon_{xz}$	$\epsilon_{first}$	$\epsilon_{third}$	$\epsilon_{int.}$	$\epsilon_{von.}$
1.	M1	140.10 4	57.809	19.569	259.625	0.745 $\times 10^{-9}$	0.738 $\times 10^{-9}$	267.986	267.986	1.266 $\times 10^{-3}$	9.45 $\times 10^{-13}$	9.36 $\times 10^{-13}$	0.255 $\times 10^{-3}$	1.307 $\times 10^{-3}$	1.307 $\times 10^{-3}$	1.307 $\times 10^{-3}$
2.	M2	140.10 4	0.53	1.336	49.866	8.682	8.602	52.803	52.084	0.243 $\times 10^{-3}$	0.11 $\times 10^{-3}$	0.109 $\times 10^{-3}$	0.629 $\times 10^{-3}$	0.255 $\times 10^{-3}$	0.261 $\times 10^{-3}$	0.267 $\times 10^{-3}$
3.	M3	140.10 4	44.608	11.271	177.549	36.054	0.03	219.19	210.766	1.581 $\times 10^{-3}$	1.436 $\times 10^{-3}$	0.431 $\times 10^{-18}$	1.583 $\times 10^{-3}$	0.63 $\times 10^{-3}$	2.303 $\times 10^{-3}$	2.614 $\times 10^{-3}$
4.	M4	140.10 4	0.948	1.663	19.503	14.812	1.878	60.332	56.361	0.270 $\times 10^{-3}$	1.1 $\times 10^{-3}$	0.937 $\times 10^{-19}$	1.266 $\times 10^{-3}$	1.968 $\times 10^{-3}$	0.858 $\times 10^{-3}$	0.794 $\times 10^{-3}$

Table 5. It shows the conclusions drawn from the data analysis and a comparison of them

Model	Materials		Density (Kg/m <sup>3</sup> )	Price Kilograms, \$	Number of Layers	Length (m)	Width (mm)		Thickness (m)		The volume of the column (m <sup>3</sup> )	Density (Kg/m <sup>3</sup> )	Weight of the column (Kg)	Total price (\$)	Difference in weight %
							W <sub>1</sub>	W <sub>2</sub>	T <sub>1</sub>	T <sub>2</sub>					
M-1	Steel		7870	3.5	1	23.1	0.1524	0.1347	0.2032	0.1855	0.1382	7870	1088	3808	-----
M-2															
M-3	T300 Carbon Fiber and	T300 carbon fiber, 40 %	1765	10	140	23.1	0.1524	0	0.140	0	0.4929	1485.4	732	2950	32.72
M-4	7901 Epoxy Resin	7901 Epoxy Resin, 60 %	1299	0.05	168	23.1	0.1524	0	0.168	0	0.5914	1485.4	879	3542	19.21

Table 5 shows the findings as well as a comparison of them using various mathematical models and their corresponding weights. In addition, the weights of the four models were compared, and the difference between the weights of the steel-made first and second models and the composite-material third and fourth models weight was determined.

#### 4 Conclusions

The ANSYS program's testing of the four models under varied loads revealed that the overall deformation value in each model was equal at (140.104 mm). The following are the most important conclusions obtained from these testing follows:

- The first model had the largest distortion along the Y axis, measuring (19.596 mm), and the greatest deformation along the X axis, measuring (57.809 mm).
- In the first model, 259,625 MPa was the greatest normal stress measured in the X-axis's direction. The largest shear stress was found in the XY plane (36.054 MPa) for the third model, and in the XZ plane (8.602 MPa) for the second model. The maximum intensity stress value for the first model was (267.986 MPa), and it also had the highest von Mises stress value.
- The results of the strains show that the third model had the highest value of the normal strain toward the X axis, as well as the maximum value of the shear strain in the XY plane, with a value of (0.001436), while the fourth model had the highest value of the shear strain in the XZ plane, with a value of

(0.00109). According to the first elastic principle strain, the third model had the maximum value at (0.00153), while the highest value of the third-second elastic principle strain was in the third model, with a value of (0.001968). The results of the tests also show that the third model had the greatest levels of intensity strain and Von Misses Strain, with values of (0.002303) and (0.002614), respectively.

- One of the most significant findings from these tests, and after examining the outcomes of the various tests, is the reduction in the weight of the structures in the third and fourth models compared to the first and second models. The third model's weight decreased by 32.72% compared to the first model's weight, which had the same load in the middle, and the fourth model's weight decreased by 19.21% compared to the second model's weight.

#### References:

[1] Yu, W.B. (2002). Variational asymptotic modeling of composite dimensionally reducible structures. Ph.D. Thesis, Aerospace Engineering, Georgia Institute of Technology, pp.1-8.

[2] Shalall, M.A. (2017). Nonlinear analysis of continuous composite beam by finite element method. Journal of Engineering and Development, 9(2): 54-69.

[3] Pai, P.J., Nayfeh, A.H. (1992). A nonlinear composite beam theory. Nonlinear Dynamics Journal, 3(4): pp.273-303. <https://doi.org/10.1007/BF00045486>

[4] Osserman R. (2010) How gateway arch got

- its shape. Nexus Netw. 12, pp.167–189.  
DOI: 10.1007/s00004-010-0030-8.
- [5] Tyas A, Pichugin AV, Gilbert M. (2015). Optimum structure to carry a uniform load between pinned supports: exact analytical solution. Proc. R. Soc. A 467, pp.1101-1120. DOI: 10.1098/rspa.2010.0376.
- [6] Ravichandran, K.; Masoudi, N.; Fadel, G.M.; Wiecek, M.M. (2019). Parametric Optimization for Structural Design Problems. In Proceedings of the International Design Engineering Technical Conferences and Computers and Information in Engineering Conference, Anaheim, CA, USA: pp.18–21. <http://dx.doi.org/10.1115/DETC2019-97860>
- [7] Karash, E.T., Sultan, J.N., Najem, M.K. (2021). The difference in the wall thickness of the helicopter structure are made of composite materials with another made of steel. Mathematical Modelling of Engineering Problems 9(2), pp.313-324. <https://doi.org/10.18280/mmep.090204>.
- [8] Najem, M.K., Karash, E.T., Sultan, J.N. (2021). The amount of excess weight from the design of an armored vehicle body by using composite materials instead of steel. Revue des Composites et des Matériaux Avancés-Journal of Composite and Advanced Materials, 32(1), <https://doi.org/10.18280/rcma.320101>.
- [9] Wahyuni, E., Istiono, H., Iranata, Data., Komara, I., (2021). Analysis of Effective Optimization of Construction Technology in Municipal Engineering Construction Projects, E3S Web of Conferences 233(34):03053 <http://dx.doi.org/10.1051/e3sconf/202123303053>.
- [10] Karash, E.T., Alsttar Sediqer, T.A., Elias Kassim, M.T. (2021). A comparison between a solid block made of concrete and others made of different composite materials. Revue des Composites et des Matériaux Avancés, 31(6): pp.341-347. <https://doi.org/10.18280/RCMA.310605>.
- [11] Mohammad Takey Elias Kassim, Emad Toma Karash, Jamal Nayief Sultan, (2023). A Mathematical Model for Non-Linear Structural Analysis Reinforced Beams of Composite Materials, Mathematical Modelling of Engineering Problems Vol. 10, No. 1, February, 2023, pp.311-333. <https://doi.org/10.18280/mmep.100137>.
- [12] Alper Ilkix, Onder Peker, Emre Karamuk, Cem Demir, and Nahit Kumbasar (2006). Axial Behavior of RC Columns Retrofitted With FRP Composites, S.T. Wasti and G. Ozcebe (eds.), Advances in Earthquake Engineering for Urban Risk Reduction, pp.301-316. [http://dx.doi.org/10.1007/1-4020-4571-9\\_20](http://dx.doi.org/10.1007/1-4020-4571-9_20)
- [13] Alper Ilki, Onder Peker, Emre Karamuk, Cem Demir, and Nahit Kumbasar, (2008). FRP Retrofit of Low and Medium Strength Circular and Rectangular Reinforced Concrete Columns, Journal of Materials in Civil Engineering 20(2): pp.169-188. [http://dx.doi.org/10.1061/\(ASCE\)0899-1561\(2008\)20:2\(169\)](http://dx.doi.org/10.1061/(ASCE)0899-1561(2008)20:2(169))
- [14] Mahesh Suresh Kumawat and L G Kalurkar (2014), "Cost Analysis of Steel-Concrete Composite Structure," Int. J. Struct. Civ. Eng. Res., vol. 3, pp.158–167. DOI: 10.18178/ijscer
- [15] Md Tanvir Hasan Fahim (2022), Composite Columns in Building Structure - A Analytical Study, Material Science Research India journal, Vol.19, No. (2) 2022, pp.84-92. <http://dx.doi.org/10.13005/msri/190206>.
- [16] C. C. Chen and N. J. Lin (2006), Analytical model for predicting axial capacity and behavior of concrete encased steel composite stub columns, J. Constr. Steel Res., vol. 62, no. 5, pp.424-433. <https://doi.org/10.1016/j.jcsr.2005.04.021>.
- [17] Liu, T.; Zhang, W.; Zhang, Y.; Wang, Q. (2018), Nonlinear Dynamics of Composite Laminated Circular Cylindrical Shell With Membranes in Thermal Environment. In Proceedings of the 14th International Conference on Multibody Systems, Nonlinear Dynamics, and Control, American Society of Mechanical Engineers, Quebec City, QC, Canada; Volume 6, p. V006T09A031. <http://dx.doi.org/10.1115/DETC2018-85058>
- [18] Yang, S.W.; Hao, Y.X.; Zhang, W.; Yang, L.; Liu, L.T. (2021), Free Vibration and Buckling of Eccentric Rotating FG-GPLRC Cylindrical Shell Using First-Order Shear Deformation Theory. Compos. Struct. 113728. <http://dx.doi.org/10.1016/j.compstruct.2021.113728>
- [19] Siriguleng, B.; Zhang, W.; Liu, T.; Liu, Y.Z. (2020), Vibration Modal Experiments and Modal Interactions of a Large Space Deployable Antenna with Carbon Fiber Material and Ring-Truss Structure. Eng.

- Struct., 207, 109932.  
<http://dx.doi.org/10.1016/j.engstruct.2019.10.9932>.
- [20] Najim, M., Sultan, J., Karash, E. (2020). Comparison of the resistance of solid shell of composite materials with other solid metal Materials. In: IMDC-SDSP 2020, pp.28-30.  
<https://doi.org/10.4108/eai.28-6-2020.2298518>.
- [21] Karash, E.T. (2011). Modelling of unilateral contact of metal and fiberglass shells. Applied Mechanics and Materials Journal, 87: pp.206-208.  
<https://doi.org/10.4028/www.scientific.net/AMM.87.20>.
- [22] Yang, S.; Hao, Y.; Zhang, W.; Yang, L.; Liu, L. (2021), Nonlinear Vibration of Functionally Graded Graphene Platelet-Reinforced Composite Truncated Conical Shell Using First-Order Shear Deformation Theory. Appl. Math. Mech.-Engl. Ed., 42, 981-998.  
<http://dx.doi.org/10.1007/s10483-021-2747-9>
- [23] S. Chen and P. Wu (2017), Analytical model for predicting axial compressive behavior of steel reinforced concrete column,” Journal of Constructional Steel Research, vol. 128, pp.649-660.
- [24] Jipeng Yu, Tianhua Zhou, Yu Zhang, and Yapeng Li (2021), Axial Compressive Performance of Steel-Reinforced Concrete Columns with Monosymmetric Cross-Shaped Steel, Advances in Civil Engineering Volume 2021, Article ID 6666996, pp.1-17.  
<https://doi.org/10.1155/2021/6666996>.
- [25] Yi Ding, Zhen Zhou, Yang Wei, and Huiwen Tian (2022), Axial compressive behavior of ultra-high performance concrete confined by high-strength transverse reinforcements, Construction and Building Materials 324(12):126518.  
<http://dx.doi.org/10.1016/j.conbuildmat.2022.126518>.
- [26] Zhang K, Gu Y, Li M, et al. (2014), Effect of rapid curing process on the properties of carbon fiber/epoxy composite fabricated using vacuum assisted resin infusion molding. Mater Design; 54: pp.624-631.  
<http://dx.doi.org/10.1016/j.matdes.2013.08.065>.
- [27] Broughton W. R., Koukoulas T., Woolliams P., et al. (2013), Assessment of nanoparticle loading and dispersion in polymeric materials using optical coherence tomography. Polym Test; 32, pp.1290-1298.  
<http://dx.doi.org/10.1016/j.polymertesting.2013.08.004>.
- [28] Amit Kumar, Kamal Sharma, and Amit Rai Dixit (2022), Tensile, flexural and interlaminar shear strength of carbon fiber reinforced epoxy composites modified by grapheme, Polymer Bulletin 80 (7), pp.1-22.  
<http://dx.doi.org/10.1007/s00289-022-04413-w>.
- [29] A. M. D´ıez-Pascual and M. Naffakh (2012), Tuning the properties of carbon fiber-reinforced poly(phenylene sulphide) laminates via incorporation of inorganic nanoparticles, Polymer Journal, vol. 53, no. 12, pp. 2369–2378.  
<http://dx.doi.org/10.1016/j.polymer.2012.04.010>.
- [30] L.-C. Tang, H. Zhang, S. Sprenger, L. Ye, and Z. Zhang (2012), Fracture mechanisms of epoxy-based ternary composites filled with rigid-soft particles, Composites Science and Technology, vol. 72, no. 5, pp.558-565.  
<http://dx.doi.org/10.1016/j.compscitech.2011.12.015>.
- [31] S. Deng, L. Ye, and K. Friedrich (2007), Fracture behaviours of epoxy nanocomposites with nano-silica at low and elevated temperatures, Journal of Materials Science, vol. 42, no. 8, pp.2766-2774.  
<http://dx.doi.org/10.1007/s10853-006-1420-x>
- [32] Fang Liu, Shiqiang Deng, and Jianing Zhang (2017), Mechanical Properties of Epoxy and Its Carbon Fiber Composites Modified by Nanoparticles, Journal of Nanomaterials Volume 2017, Article ID 8146248, pp.1-9  
<https://doi.org/10.1155/2017/8146248>.
- [33] Hossein Rahmani, S. Heydar Mahmoudi Najafi and Alireza Ashori (2014), Mechanical performance of epoxy/carbon fiber laminated composites, Journal of Reinforced Plastics and Composites 2014, Vol. 33(8): pp.733-740. DOI: 10.1177/0731684413518255  
jrp.sagepub.com

### **Nomenclature and Greek symbols**

$S$  = Displacement

$\delta$  = Deformed and unreformed

$U_x$  = Component of the displacement ( $x$  – direction)

$U_y$  = Component of the displacement ( $y$  – direction)

$U_z$  = Component of the displacement ( $z$  – direction)

$\sigma_x$  = Normal stress

$\tau_{xy}$  = shear stress

$\tau_{xz}$  = shear stress

$\sigma_{int.}$  = Stress intensity

$\sigma_{von}$  = Von mises stress

$\varepsilon_x$  = Normal strain ( $x$  – direction)

$\varepsilon_{xy}$  = Shear strain ( $xy$  – direction)

$\varepsilon_{xz}$  = Shear strain ( $xz$  – direction)

$\varepsilon_{first}$  = First principal elastic strain

$\varepsilon_{third}$  = Third principal elastic strain

$\varepsilon_{intensity}$  = Elastic strain intensity

$\varepsilon_{von}$  = Von mises elastic strain

### **Contribution of Individual Authors to the Creation of a Scientific Article (Ghostwriting Policy)**

The authors equally contributed in the present research, at all stages from the formulation of the problem to the final findings and solution.

### **Sources of Funding for Research Presented in a Scientific Article or Scientific Article Itself**

No funding was received for conducting this study.

### **Conflict of Interest**

The authors have no conflict of interest to declare.

### **Creative Commons Attribution License 4.0 (Attribution 4.0 International, CC BY 4.0)**

This article is published under the terms of the Creative Commons Attribution License 4.0

[https://creativecommons.org/licenses/by/4.0/deed.en\\_US](https://creativecommons.org/licenses/by/4.0/deed.en_US)